

Observational constraints on dynamical dark energy with pivoting redshift

Weiqliang Yang,^{1,*} Supriya Pan,^{2,†} Eleonora Di Valentino,^{3,‡} and Emmanuel N. Saridakis^{4,5,§}

¹*Department of Physics, Liaoning Normal University, Dalian, 116029, P. R. China*

²*Department of Mathematics, Presidency University, 86/1 College Street, Kolkata 700073, India*

³*Jodrell Bank Center for Astrophysics, School of Physics and Astronomy,
University of Manchester, Oxford Road, Manchester, M13 9PL, UK*

⁴*Department of Physics, National Technical University of Athens, Zografou Campus GR 157 73, Athens, Greece*

⁵*CASPER, Physics Department, Baylor University, Waco, TX 76798-7310, USA*

We investigate the generalized Chevallier-Polarski-Linder (CPL) parametrization, which contains the pivoting redshift z_p as an extra free parameter. We use various data combinations from cosmic microwave background (CMB), baryon acoustic oscillations (BAO), redshift space distortion (RSD), weak lensing (WL), joint light curve analysis (JLA), cosmic chronometers (CC), and we include a Gaussian prior on the Hubble constant value, in order to extract the observational constraints on various quantities. For the case of free z_p we find that for all data combinations it always remains unconstrained, and there is a degeneracy with the current value of the dark energy equation of state w_0 . For the case where z_p is fixed to specific values, and for the full data combination, we find that with increasing z_p the mean value of w_0 slowly moves into the phantom regime, however the cosmological constant is always allowed within 1σ confidence-level. However, the significant effect is that with increasing z_p the correlations between w_0 and w_a change from negative to positive, with the case $z_p = 0.35$ corresponding to no correlation. This feature indeed justifies why a non-zero pivoting redshift should be taken into account.

PACS numbers: 98.80.-k, 95.36.+x, 95.35.+d, 98.80.Es

I. INTRODUCTION

According to observations the universe has entered a period of accelerated expansion in the recent cosmological past. In order to provide an explanation, physicists follow two main directions. The first is to maintain general relativity as the gravitational theory and introduce new, exotic fluids in the universe content, dubbed as dark energy sector [1, 2]. The second way is to modify the gravitational sector, constructing extended theories of gravity that possess general relativity as a particular limit but which in general present extra degrees of freedom, capable of describing the universe behavior [3, 4, 5, 6, 7].

However, both approaches can be quantified by the introduction of an equation-of-state parameter for the dark energy perfect fluid (effective in the case of modified gravity), namely $w_x(z) = p_x(z)/\rho_x(z)$, where $p_x(z)$, $\rho_x(z)$ are respectively the pressure and the energy density. Hence, introducing various parametrizations of $w_x(z)$ allows us to describe the universe evolution in a phenomenological way, even if the microphysical origin of the cause of acceleration is unknown. Following this, a large number of parametrizations have been introduced in the last years, namely the one-parameter dark energy parametrizations [8, 9], or the two-parameters family, such as the Chevallier-Polarski-Linder (CPL)

parametrization [10, 11], the Linear parametrization [12, 13, 14], the Logarithmic parametrization [15], the Jassal-Bagla-Padmanabhan parametrization (JBP) [16], the Barboza-Alcaniz (BA) parametrization [17], etc (see for instance [18, 19, 20, 21, 22, 23, 24, 25, 26, 27, 28, 29, 30, 31, 32, 33, 34, 35, 36, 37, 38, 39, 40, 41, 42] and references therein).

In most of the above dark-energy equation-of-state parametrizations one considers the “pivoting redshift” to correspond to zero, namely the point in which w_x is most tightly constrained to correspond to the current universe. However, due to possible rotational correlations between the two parameters of the two-parameter models, in principle one could avoid setting the pivoting redshift to zero straightaway, and let it as a free parameter [43, 44].

In the present work we are interested in investigating the observational constraints on the most well-known parametrization, namely the CPL one, incorporating however the pivoting redshift as an extra parameter, assuming it to be either fixed or free. A first examination towards this direction was performed in [45], however in the present work we provide a robust analysis with the latest cosmological data. In particular, we will use data from cosmic microwave background (CMB), baryon acoustic oscillations (BAO), redshift space distortion (RSD), weak lensing (WL), joint light curve analysis (JLA), cosmic chronometers (CC), while we will include a Gaussian prior on the Hubble constant value.

The plan of the work is the following: In Section II we present the basic equations of a parametrized dark energy model at the background and perturbative levels. Section III describes the various data sets used in this work. In Section IV we perform the observational

*Electronic address: d11102004@163.com

†Electronic address: supriya.maths@presiuniv.ac.in

‡Electronic address: eleonora.divalentino@manchester.ac.uk

§Electronic address: Emmanuel.Saridakis@baylor.edu

confrontation, extracting the constraints on the model parameters and on various cosmological quantities. Finally, we summarize the obtained results in Section VI.

II. DYNAMICAL DARK-ENERGY WITH PIVOTING REDSHIFT

In this section we briefly review the basic equations for a non-interacting cosmological scenario both at background and perturbative levels, and we introduce the pivoting redshift dark energy parametrization. We consider the homogeneous and isotropic Friedmann-Lemaître-Robertson-Walker (FLRW) line element

$$ds^2 = -dt^2 + a^2(t) \left[\frac{dr^2}{1 - Kr^2} + r^2 (d\theta^2 + \sin^2 \theta d\phi^2) \right], \quad (1)$$

where $a(t)$ is the scale factor and $K = -1, +1, 0$ corresponds to open, closed and flat geometry, respectively. Additionally, we consider that the universe is filled with baryons, cold dark matter, radiation, and the (effective) dark energy fluid. Hence, the evolution of the universe is determined by the Friedmann equations, which are written as

$$H^2 + \frac{K}{a^2} = \frac{8\pi G}{3} \rho_{tot}, \quad (2)$$

$$2\dot{H} + 3H^2 + \frac{K}{a^2} = -8\pi G p_{tot}, \quad (3)$$

where G is the Newton's gravitational constant and $H = \dot{a}/a$ is the Hubble function, with dots denoting derivatives with respect to the cosmic time t . Moreover, in the above equations we have introduced the total energy density and pressure of the universe, reading as $\rho_{tot} = \rho_r + \rho_b + \rho_c + \rho_x$ and $p_{tot} = p_r + p_b + p_c + p_x$, with the symbols r, b, c, x corresponding to radiation, baryon, cold dark matter and dark energy fluid, respectively. In the following we focus our analysis on the spatially flat case ($K = 0$), which is the one favored by observations.

In the case where the above sectors do not present mutual interactions, we can write the conservation equation of each fluid as

$$\dot{\rho}_i + 3H(1 + w_i)\rho_i = 0, \quad (4)$$

where $w_i \equiv p_i/\rho_i$ is known as the equation-of-state parameter of the i -th fluid ($i \in \{r, b, c, x\}$). In the case of the dark energy fluid, the solution of (4) is

$$\rho_x = \rho_{x,0} \left(\frac{a}{a_0} \right)^{-3} \exp \left[-3 \int_{a_0}^a \frac{w_x(a')}{a'} da' \right], \quad (5)$$

where $\rho_{x,0}$ is the current value of ρ_x and a_0 is the present value of the scale factor which is set to unity.

From expression (5) we deduce that the evolution of the dark energy component is highly dependent on the form of its equation-of-state parameter $w_x(a)$. In the simplest case where $w_x(a) = w_0 = \text{const.}$ the dark energy

fluid evolves as $\rho_x = \rho_{x,0} a^{-3(1+w_0)}$. Nevertheless, for dynamical $w_x(a)$ one may consider various parametrizations in terms of the scale factor or the redshift z , where $1 + z = a_0/a = 1/a$. Thus, in the literature one can find many forms of such parametrizations.

One of the well known parametrizations of the dark-energy equation-of-state parameter is the Chevallier-Polarski-Linder (CPL) one, given by [10, 11]

$$w_x(z) = w_0 + w_a(1 - a), \quad (6)$$

where w_0 is the current value of w_x and $w_a \equiv dw_x/da$ at $a = a_0 = 1$. One can see that introducing an extra parameter, expression (6) can be rewritten as

$$w_x(z) = w_0^p + w_a^p(a_p - a), \quad (7)$$

where $w_0^p = w_0 - w_a(1 - a_p)$, $w_a^p = w_a$ and $1 + z_p = 1/a_p$. In the case where the extra parameter $z_p = 0$, we obtain $a_p = 1$, and thus we recover the standard CPL model (6). The parameter z_p is called the ‘‘pivoting redshift’’ with a_p its corresponding scale factor, since it marks the point in which w_x is most tightly constrained [43, 44]. In particular, it is known that in the above parametrization z_p , and thus w_0^p , depend on the probing method, the fiducial scenario, and the imposed priors [43]. Hence, in principle one could avoid setting $z_p = 0$ straightaway, and let it as a free parameter. Thus, w_0^p can be more precisely determined than w_0 , and actually it is indeed the most precisely determined value of $w_x(z)$. In this work we are interested in investigating the generalized CPL parametrization (7), namely incorporating the pivoting redshift as an extra parameter, assuming it to be either fixed or free.

We proceed by providing the cosmological equations at the perturbation level. In the synchronous gauge the perturbed FLRW metric reads as

$$ds^2 = a^2(\tau) [-d\tau^2 + (\delta_{ij} + h_{ij})dx^i dx^j], \quad (8)$$

where δ_{ij} is the unperturbed and h_{ij} the perturbed metric, and τ is the conformal time. Using the above perturbed metric one can solve the conservation equations $T_{;\nu}^{\mu\nu} = 0$. Thus, for a mode with wavenumber k the perturbed equations can be written as [46, 47, 48]

$$\begin{aligned} \delta'_i &= -(1 + w_i) \left(\theta_i + \frac{h'}{2} \right) - 3\mathcal{H} \left(\frac{\delta p_i}{\delta \rho_i} - w_i \right) \delta_i \\ &\quad - 9\mathcal{H}^2 \left(\frac{\delta p_i}{\delta \rho_i} - c_{a,i}^2 \right) (1 + w_i) \frac{\theta_i}{k^2}, \end{aligned} \quad (9)$$

$$\theta'_i = -\mathcal{H} \left(1 - 3 \frac{\delta p_i}{\delta \rho_i} \right) \theta_i + \frac{\delta p_i / \delta \rho_i}{1 + w_i} k^2 \delta_i - k^2 \sigma_i, \quad (10)$$

where primes denote derivatives with respect to the conformal time, and $\mathcal{H} = a'/a$ is the conformal Hubble factor. Additionally, $\delta_i = \delta \rho_i / \rho_i$ is the density perturbation for the i -th fluid, $\theta_i \equiv ik^j v_j$ is the divergence of the i -th fluid velocity, $h = h_j^j$ is the trace of the metric perturbations h_{ij} , and σ_i is the anisotropic stress of the i -th fluid.

Note that in the following we set $\sigma_i \equiv 0$ for all i , since we assume zero anisotropic stress for all fluids. Finally, $c_{a,i}^2 = \dot{p}_i/\dot{\rho}_i$ is the adiabatic speed of sound of the i -th fluid, and it is given by $c_{a,i}^2 = w_i - \frac{w'_i}{3\mathcal{H}(1+w_i)}$ in the case where we set the sound speed $c_s^2 = \delta p_i/\delta \rho_i$ to 1.

III. OBSERVATIONAL DATA

In this section we present the various observational data set that are going to be used in order to confront dark energy parametrizations with pivoting redshift. In our analysis we incorporate the data by varying nine cosmological parameters: the baryon energy density $\Omega_b h^2$, the cold dark matter energy density $\Omega_c h^2$, the ratio between the sound horizon and the angular diameter distance at decoupling Θ_s , the reionization optical depth τ , the spectral index of the scalar perturbations n_s , the amplitude of the primordial power spectrum A_s , the two parameters of the CPL parametrization w_0 and w_a and the pivot z_p . Furthermore, we explore all parameters within the range of the conservative flat priors shown in Table I.

Parameter	Prior
$\Omega_b h^2$	[0.005, 0.1]
$\Omega_c h^2$	[0.01, 0.99]
τ	[0.01, 0.8]
n_s	[0.5, 1.5]
$\log[10^{10} A_s]$	[2.4, 4]
$100\theta_{MC}$	[0.5, 10]
w_0	[-2, 0]
w_a	[-3, 3]
z_p	[0, 5]

TABLE I: The flat priors on the cosmological parameters used in the present analyses.

Let us now present in detail the data sets that we will use.

- **Cosmic microwave background (CMB):** We constrain the parameters by analyzing the full range of the 2015 Planck temperature and polarization power spectra ($2 \leq \ell \leq 2500$) [49, 50]. This dataset is identified as the Planck TTTEEE+lowTEB. At the time of writing only the Planck 2015 likelihood was publicly available, however we do not expect the conclusions of this paper to change significantly given the similarities between Planck 2015 and Planck 2018 results [51, 52].
- **Baryon acoustic oscillations (BAO):** We consider the baryon acoustic oscillations as was done in [53]. They are the 6dF Galaxy Survey (6dFGS) measurement at $z_{\text{eff}} = 0.106$ [54], the Main Galaxy

Sample of Data Release 7 of Sloan Digital Sky Survey (SDSS-MGS) at $z_{\text{eff}} = 0.15$ [55], and the CMASS and LOWZ samples from the Data Release 12 (DR12) of the Baryon Oscillation Spectroscopic Survey (BOSS) at $z_{\text{eff}} = 0.57$ and at $z_{\text{eff}} = 0.32$ [56].

- **Redshift space distortion (RSD):** We add two redshift space distortion data. In particular, we include the data from CMASS and LowZ galaxy samples. The CMASS sample consists of 777202 galaxies having the effective redshift of $z_{\text{eff}} = 0.57$ [57], whereas the LOWZ sample consists of 361762 galaxies having an effective redshift of $z_{\text{eff}} = 0.32$ [57].
- **Weak lensing (WL):** We include the cosmic shear data from the Canada–France–Hawaii Telescope Lensing Survey (CFHTLenS) [58, 59, 60].
- **Joint light curve analysis (JLA):** We consider the joint light curve analysis sample [61] consisting of 740 luminosity distance measurements of Supernovae Type Ia data in the redshift interval $z \in [0.01, 1.30]$.
- **Cosmic chronometers (CC):** We add the thirty measurements of the cosmic chronometers in the redshift interval $0 < z < 2$. The CC data have been summarized in [62].
- We include a Gaussian prior on the Hubble constant value from Riess et al. [63] (i.e. $H_0 = 73.24 \pm 1.75 \text{ km s}^{-1} \text{ Mpc}^{-1}$), referred as HST.

In order to incorporate statistically the several combinations of datasets and extract the observational constraints, we use our modified version of the publicly available Monte-Carlo Markov Chain package *Cosmomc* [64], which is an efficient Monte Carlo algorithm equipped with a convergence diagnostic based on the Gelman and Rubin statistic [65]. It implements an efficient sampling of the posterior distribution using the fast/slow parameter decorrelations [66] and additionally it includes the support for the Planck data release 2015 Likelihood Code [50]¹.

¹ This code is publicly available at <http://cosmologist.info/cosmomc/>.

Parameters	CMB	CBR	CBH	CBRWJCH
$\Omega_c h^2$	0.1191 ± 0.0014	0.1192 ± 0.0013	0.1194 ± 0.0013	0.1183 ± 0.0012
$\Omega_b h^2$	0.02228 ± 0.00016	$0.02226^{+0.00014}_{-0.00016}$	0.02226 ± 0.00015	0.02231 ± 0.00015
$100\theta_{MC}$	1.04080 ± 0.00033	$1.04077^{+0.00032}_{-0.00031}$	1.04076 ± 0.00033	1.04088 ± 0.00031
τ	0.076 ± 0.018	0.074 ± 0.017	0.078 ± 0.018	0.064 ± 0.017
n_s	0.9665 ± 0.0045	$0.9661^{+0.0045}_{-0.0042}$	$0.9658^{+0.0046}_{-0.0045}$	0.9676 ± 0.0044
$\ln(10^{10} A_s)$	3.085 ± 0.034	3.081 ± 0.034	3.089 ± 0.034	3.058 ± 0.033
w_0	< -1.3	$-1.33^{+0.35}_{-0.31}$	$-1.19^{+0.20}_{-0.11}$	$-1.11^{+0.17}_{-0.11}$
w_a	$-0.5^{+1.2}_{-2.0}$	$-1.21^{+0.62}_{-0.62}$	$-0.25^{+0.57}_{-0.47}$	$-0.24^{+0.38}_{-0.33}$
z_p	unconstrained	unconstrained	unconstrained	unconstrained
Ω_{m0}	$0.217^{+0.026}_{-0.076}$	0.340 ± 0.017	$0.291^{+0.014}_{-0.015}$	$0.3011^{+0.0080}_{-0.0081}$
σ_8	$0.96^{+0.11}_{-0.06}$	0.804 ± 0.016	$0.854^{+0.020}_{-0.021}$	$0.819^{+0.014}_{-0.013}$
H_0	83^{+14}_{-8}	$64.7^{+1.5}_{-1.7}$	$70.0^{+1.7}_{-1.8}$	$68.52^{+0.85}_{-0.91}$
χ^2_{\min} (best-fit)	12960.50	12969.720	12975.612	13723.308

TABLE II: Summary of the 68% CL constraints on the generalized CPL parametrization (7), in the case where the pivoting redshift z_p is handled as a free parameter, using various combinations of the observational data sets. Here, CBR = CMB+BAO+RSD, CBH = CMB+BAO+HST, and CBRWJCH = CMB+BAO+RSD+WL+JLA+CC+HST.

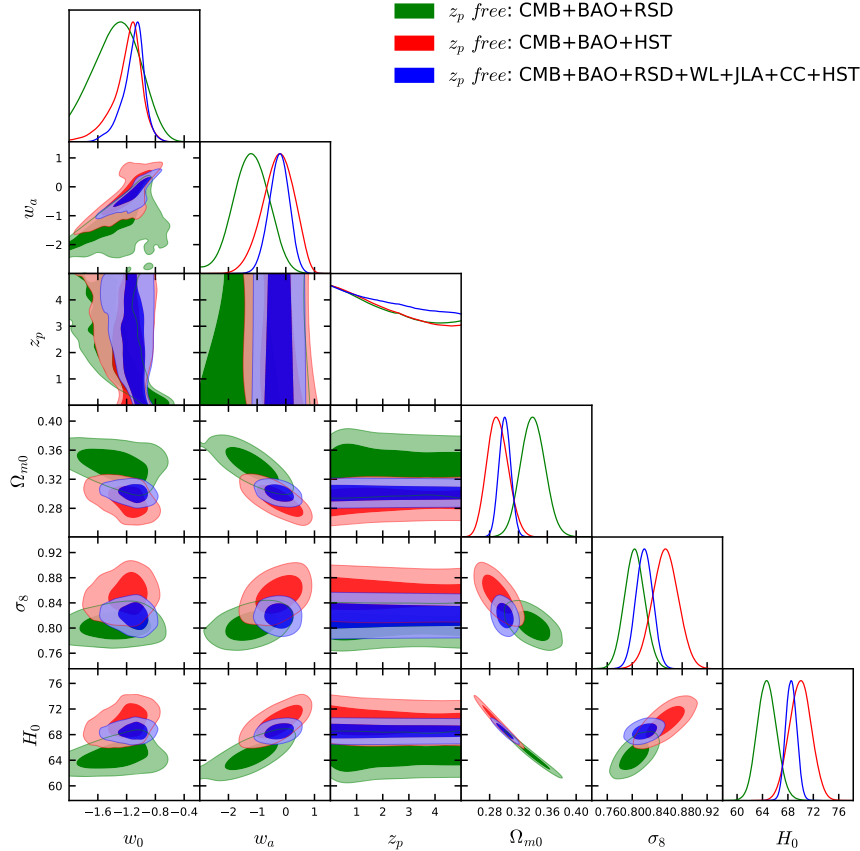


FIG. 1: The 68% and 95% CL 2-dimensional (2D) contour plots for several combinations of various quantities and using various combinations of the observational data sets, for the generalized CPL parametrization (7) in the case where the pivoting redshift z_p is handled as a free parameter, and the corresponding 1-dimensional (1D) marginalized posterior distributions.

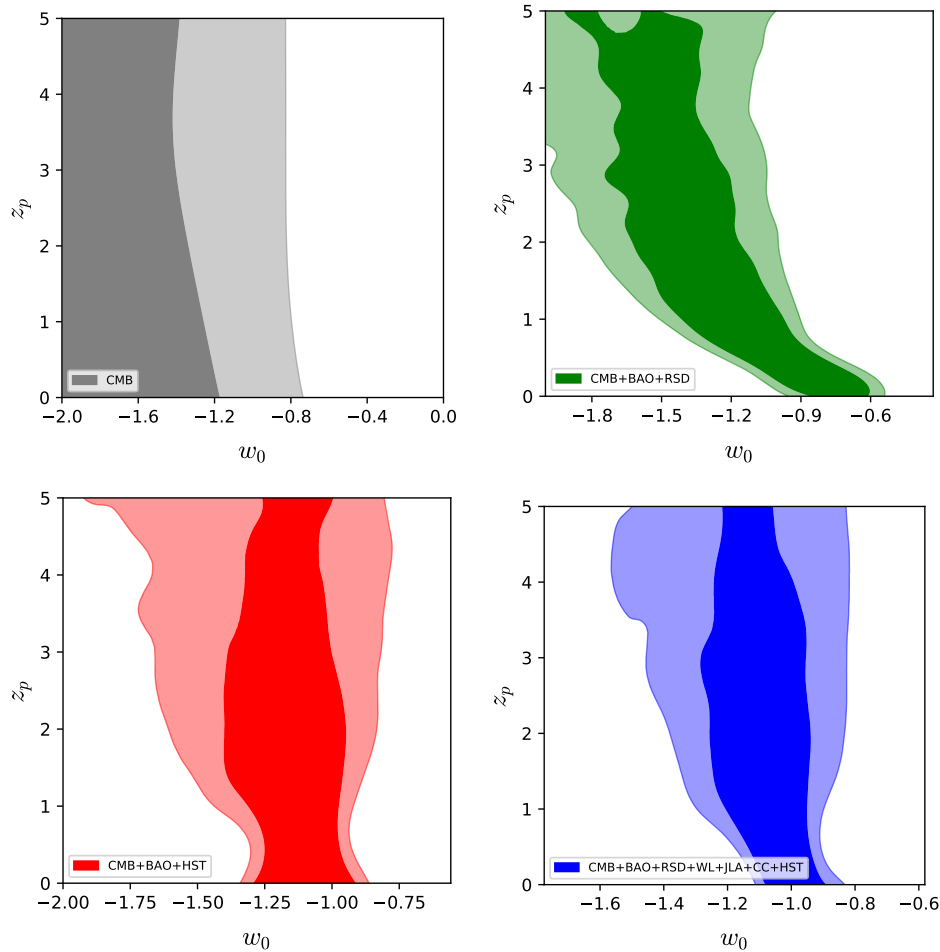


FIG. 2: 68% and 95% CL contour plots in the $w_0 - z_p$ plane using various combinations of the observational data sets, for the generalized CPL parametrization (7) in the case where the pivoting redshift z_p is handled as a free parameter.

IV. OBSERVATIONAL CONSTRAINTS

In this section we provide the observational constraints on the generalized CPL parametrization with pivoting redshift. We consider two separate cosmological scenarios, namely one where the pivoting redshift is handled as a free parameter, and one where we fix the pivoting redshift to specific values in the region $z_p \in [0, 1]$. Moreover, in order to acquire a complete picture of the behavior of the scenario, we consider different combinations of the observational datasets described above.

A. Pivoting redshift as a free parameter

We desire to impose observational constraints on the generalized CPL parametrization (7), handling the pivoting redshift z_p as a free parameter. The results of the analysis can be seen in Table II, where we display the 68% (1σ) confidence level (CL) constraints for various quantities, while the full contour plots are presented in

Fig. 1.

For the case where only CMB data are used, the Hubble constant value H_0 at present increases and its error bars are strikingly large ($H_0 = 83_{-8}^{+14}$ at 68% CL). Moreover, the present value of the dark-energy equation-of-state parameter is found to lie deeply in the phantom region, with $w_0 < -1.3$ at 68% CL.

When the BAO and RSD data are added to CMB (shown in Table II as the CBR combination), H_0 decreases ($H_0 = 64.7_{-1.7}^{+1.5}$ at 68% CL) as well as its error bar, while the matter density increases significantly ($\Omega_{m0} = 0.340 \pm 0.017$ at 68% CL). Additionally, in this data combination we obtain changes into the dark energy constraints. In particular, although the mean value of the current dark energy equation-of-state parameter is in the phantom regime ($w_0 = -1.33_{-0.31}^{+0.35}$) at 68% CL, the quintessence regime is allowed too, in contrast to the constraints from CMB only.

When the BAO and the HST data are added to CMB (i.e. the combined analysis CMB+BAO+HST called CBH in Table II), the value of H_0 increases

Parameters	CMB	CBR	CBH	CBRWJCH
$\Omega_c h^2$	$0.1190^{+0.0013}_{-0.0013}$	$0.1192^{+0.0013}_{-0.0013}$	$0.1193^{+0.0014}_{-0.0014}$	$0.1181^{+0.0011}_{-0.0012}$
$\Omega_b h^2$	$0.02229^{+0.00015}_{-0.00017}$	$0.02226^{+0.00015}_{-0.00015}$	$0.02226^{+0.00015}_{-0.00017}$	$0.02233^{+0.00016}_{-0.00015}$
$100\theta_{MC}$	$1.04079^{+0.00033}_{-0.00033}$	$1.04076^{+0.00031}_{-0.00031}$	$1.04076^{+0.00032}_{-0.00033}$	$1.04089^{+0.00031}_{-0.00031}$
τ	$0.077^{+0.016}_{-0.016}$	$0.074^{+0.016}_{-0.016}$	$0.079^{+0.018}_{-0.017}$	$0.066^{+0.017}_{-0.018}$
n_s	$0.9668^{+0.0044}_{-0.0044}$	$0.9662^{+0.0045}_{-0.0044}$	$0.9660^{+0.0043}_{-0.0043}$	$0.9682^{+0.0042}_{-0.0043}$
$\ln(10^{10} A_s)$	$3.087^{+0.035}_{-0.032}$	$3.081^{+0.032}_{-0.032}$	$3.090^{+0.034}_{-0.033}$	$3.061^{+0.033}_{-0.034}$
w_0	$-1.28^{+0.34}_{-0.44}$	$-0.68^{+0.24}_{-0.19}$	$-1.05^{+0.13}_{-0.18}$	$-1.001^{+0.061}_{-0.078}$
w_a	$-0.9^{+1.4}_{-1.2}$	$-1.10^{+0.70}_{-0.92}$	$-0.20^{+0.61}_{-0.41}$	$-0.09^{+0.32}_{-0.20}$
Ω_{m0}	$0.226^{+0.036}_{-0.084}$	$0.337^{+0.019}_{-0.020}$	$0.290^{+0.013}_{-0.017}$	0.3001 ± 0.0078
σ_8	$0.95^{+0.12}_{-0.08}$	$0.805^{+0.016}_{-0.016}$	$0.854^{+0.022}_{-0.022}$	$0.819^{+0.014}_{-0.014}$
H_0	81^{+14}_{-10}	$65.0^{+1.7}_{-1.9}$	$70.1^{+2.0}_{-1.7}$	$68.58^{+0.85}_{-0.83}$
χ^2_{\min} (best-fit)	12961.940	12971.976	12976.132	13724.29

TABLE III: Summary of the 68% CL constraints on the generalized CPL parametrization (7), in the case where the pivoting redshift is fixed at $z_p = 0.05$, using various combinations of the observational data sets. Here, CBR = CMB+BAO+RSD, CBH = CMB+BAO+HST, and CBRWJCH = CMB+BAO+RSD+WL+JLA+CC+HST.

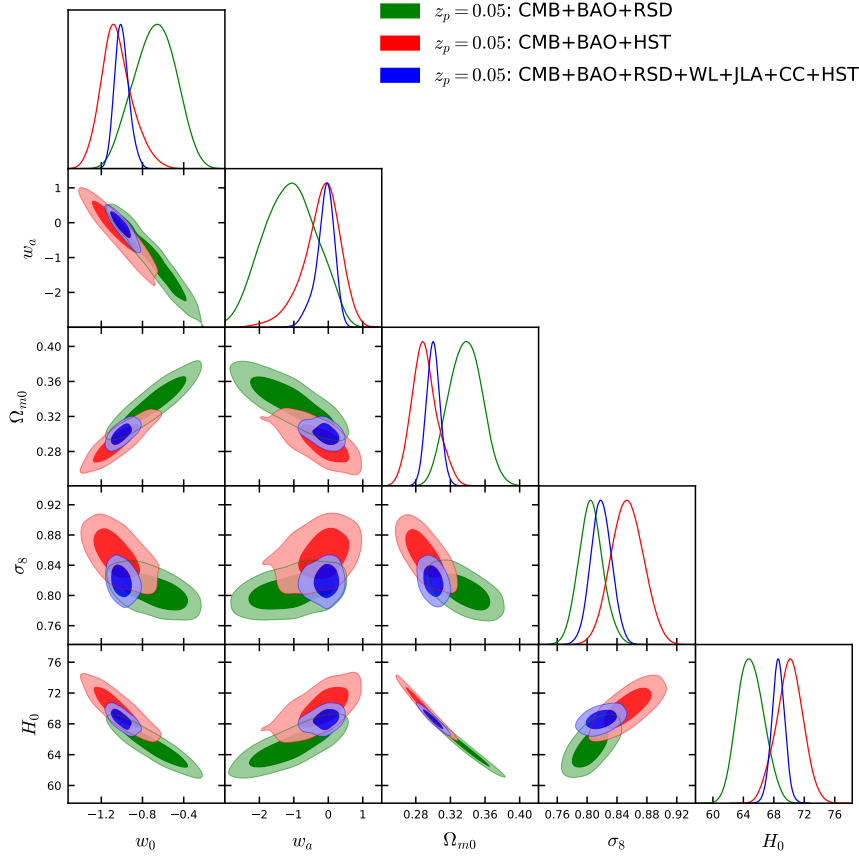


FIG. 3: The 68% and 95% CL 2D contour plots for several combinations of various quantities and using various combinations of the observational data sets, for the generalized CPL parametrization (7) in the case where the pivoting redshift is fixed at $z_p = 0.05$, and the corresponding 1D marginalized posterior distributions.

again. Concerning w_0 we also see that a phantom mean value is favored, nevertheless the quintessence regime is allowed within 1σ . In addition, the parameter w_a increases significantly in comparison to its CMB and

CMB+BAO+RSD constraints. However, as can be seen in Fig. 1, note that the contour plots of the combination of CMB+BAO+RSD data (green contours) are in tension with CMB+BAO+HST ones (red contours).

Parameters	CMB	CBR	CBH	CBRWJCH
$\Omega_c h^2$	$0.1191^{+0.0014}_{-0.0015}$	$0.1191^{+0.0013}_{-0.0014}$	$0.1193^{+0.0013}_{-0.0013}$	$0.1181^{+0.0012}_{-0.0013}$
$\Omega_b h^2$	$0.02228^{+0.00015}_{-0.00015}$	$0.02225^{+0.00015}_{-0.00015}$	$0.02225^{+0.00014}_{-0.00014}$	$0.02234^{+0.00015}_{-0.00015}$
$100\theta_{MC}$	$1.04080^{+0.00031}_{-0.00031}$	$1.04077^{+0.00032}_{-0.00033}$	$1.04076^{+0.00031}_{-0.00031}$	$1.04090^{+0.00031}_{-0.00030}$
τ	$0.078^{+0.018}_{-0.017}$	$0.075^{+0.018}_{-0.018}$	$0.078^{+0.017}_{-0.017}$	$0.066^{+0.018}_{-0.018}$
n_s	$0.9665^{+0.0044}_{-0.0044}$	$0.9661^{+0.0044}_{-0.0044}$	$0.9659^{+0.0045}_{-0.0045}$	$0.9682^{+0.0040}_{-0.0041}$
$\ln(10^{10} A_s)$	$3.088^{+0.035}_{-0.033}$	$3.082^{+0.037}_{-0.033}$	$3.090^{+0.034}_{-0.033}$	$3.061^{+0.034}_{-0.034}$
w_0	$-1.25^{+0.33}_{-0.43}$	$-0.78^{+0.12}_{-0.16}$	$-1.05^{+0.09}_{-0.12}$	$-1.010^{+0.045}_{-0.053}$
w_a	$-0.7^{+1.3}_{-1.1}$	$-1.05^{+0.92}_{-0.59}$	$-0.27^{+0.64}_{-0.39}$	$-0.09^{+0.30}_{-0.19}$
Ω_{m0}	$0.25^{+0.05}_{-0.10}$	$0.336^{+0.017}_{-0.021}$	$0.291^{+0.013}_{-0.016}$	$0.3001^{+0.0076}_{-0.0078}$
σ_8	$0.92^{+0.11}_{-0.10}$	$0.806^{+0.016}_{-0.016}$	$0.854^{+0.020}_{-0.021}$	$0.819^{+0.014}_{-0.014}$
H_0	78^{+10}_{-15}	$65.1^{+1.8}_{-1.7}$	70.0 ± 1.7	$68.60^{+0.80}_{-0.90}$
χ^2_{\min} (best-fit)	12961.990	12970.624	12978.076	13723.892

TABLE IV: Summary of the 68% CL constraints on the generalized CPL parametrization (7), in the case where the pivoting redshift is fixed at $z_p = 0.15$, using various combinations of the observational data sets. Here, CBR = CMB+BAO+RSD, CBH = CMB+BAO+HST, and CBRWJCH = CMB+BAO+RSD+WL+JLA+CC+HST.

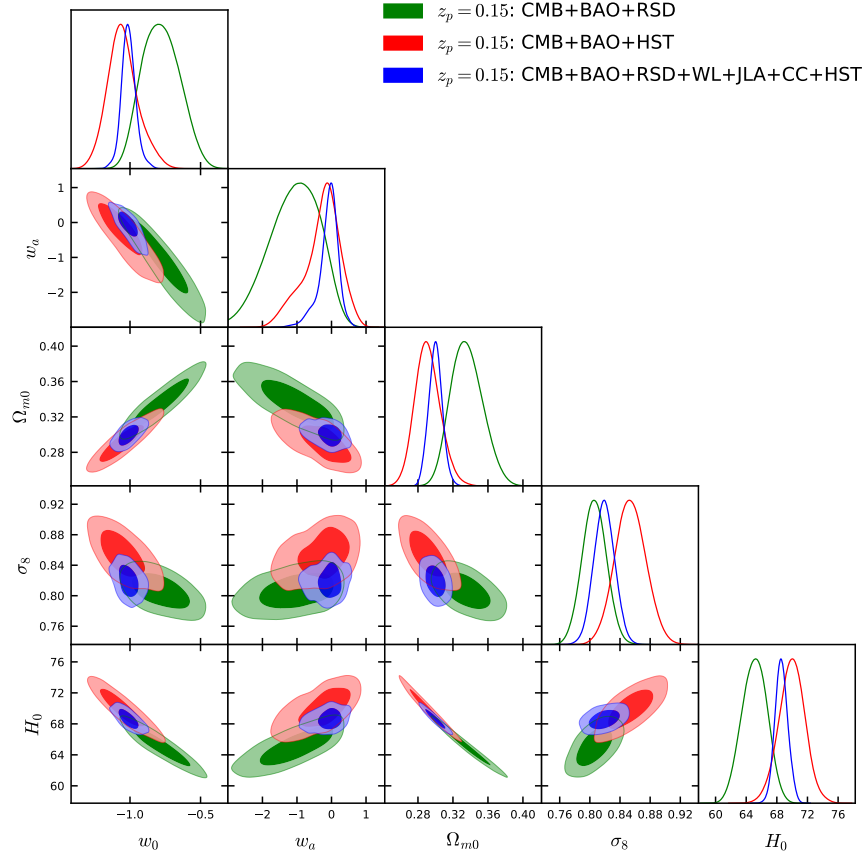


FIG. 4: The 68% and 95% CL 2D contour plots for several combinations of various quantities and using various combinations of the observational data sets, for the generalized CPL parametrization (7) in the case where the pivoting redshift is fixed at $z_p = 0.15$, and the corresponding 1D marginalized posterior distributions.

Finally, for the full analysis with all data sets (i.e. CMB+BAO+RSD+WL+JLA+CC+HST named collectively as CBRWJCH), summarized in the last column of Table II, we find that the error bars on H_0 decrease

compared to the other three analyses. Furthermore, the value of w_0 is in agreement with the cosmological constant within 1σ , which can also be seen in Fig. 1.

As we observe, for all combinations of data used,

the pivoting redshift remains unconstrained in the range $[0, 5]$, since z_p remains uncorrelated with most of the cosmological parameters, with the exception of the current dark-energy equation of state w_0 . In order to provide the latter behavior in a clearer way in Fig. 2 we present the corresponding contour plots in the $w_0 - z_p$ plane. Hence, it is of great importance to examine the cosmological constraints on the generalized CPL model, handling z_p as a fixed parameter, but still with a value different than $z_p = 0$ which is its standard CPL value. This is performed in the next subsection.

B. Fixed pivoting redshifts

In this subsection we proceed to the investigation of the generalized CPL parametrization (7), handling z_p as a fixed parameter in the range $[0, 1]$. In particular, we consider six different values of z_p , namely $z_p = 0.05, 0.15, 0.25, 0.35, 0.50$ and 1 , in order to examine how the observational constraints will change. Moreover, to be uniform we consider the same data combinations with the previous subsection.

1. Pivoting redshift $z_p = 0.05$

We begin our analysis choosing a very small value $z_p = 0.05$ and we perform the observational fittings considering several data combinations. The results are summarized in Table III and the 68% and 95% CL contour plots are displayed in Fig. 3.

In the case where we use the CMB data only, the current Hubble constant acquires a large value $H_0 = 81^{+14}_{-10}$ (at 68% CL), with significantly large error bars. Concerning the current value of the dark-energy equation-of-state parameter w_0 , its mean value lies in the phantom regime ($w_0 = -1.28^{+0.34}_{-0.44}$ at 68% CL), nevertheless it is consistent with the cosmological constant within one standard deviation.

In the case where we include BAO and RSD to CMB data (this combination is named as CBR in Table III) we obtain lower H_0 values ($H_0 = 65.0^{+1.7}_{-1.9}$ at 68% CL) and its error bars are significantly reduced. Moreover, w_0 lies in the quintessence regime in more than 1σ ($w_0 = -0.68^{+0.24}_{-0.19}$ at 68% CL), however w_a appears to be different from zero at more than one standard deviation ($w_a = -1.10^{+0.70}_{-0.92}$ at 68% CL), due to its strong anti-correlation with w_0 . Finally, for this data combination the matter density parameter at present is rather large ($\Omega_{m0} = 0.337^{+0.019}_{-0.020}$ at 68% CL) compared to the Planck 2015 results [67].

On the other hand, including BAO and HST to CMB data (this combination is denoted as CBH in Table III) H_0 decreases with respect to the sole CMB case ($H_0 = 70.0^{+2.0}_{-1.7}$ at 68% CL), but it acquires a higher value with respect to the dataset CBR, in a similar way to what we observed in the free z_p analysis presented in section IV A. Additionally, w_0 is in agreement with the cosmological constant value at 68% CL, and similarly, the parameters w_0 , w_a , and Ω_{m0} are in better agreement with the Planck 2015 findings comparing to the previous data combination CBR above.

Finally, the full combined analysis CMB+BAO+RSD+WL+JLA+CC+HST produces stronger constraints on the parameters, and the results are in significantly better agreement with Λ CDM cosmology. Concerning the dark-energy equation-of-state parameter we obtain $w_0 = -1.001^{+0.061}_{-0.078}$ and $w_a = -0.09^{+0.32}_{-0.20}$ at 68% CL.

2. Pivoting redshift $z_p = 0.15$

We proceed to the case where the pivot redshift is fixed to a slightly larger value, namely $z_p = 0.15$. The results of the observational confrontation for various datasets are summarized in Table IV, and the 68% and 95% CL contour plots are presented in Fig. 4.

For the case of CMB data only the increased z_p , comparing to the analysis of the previous paragraph, leads to smaller H_0 values ($H_0 = 78^{+10}_{-15}$ at 68% CL). On the other hand, w_0 and Ω_{m0} increase in comparison to the previous, $z_p = 0.05$, analysis.

In the combined analysis CMB+BAO+RSD we also see that w_0 is slightly shifted towards the cosmological constant comparing to the $z_p = 0.05$ case. Furthermore, for the last two combinations of datasets, namely, CMB+BAO+HST (CBH in Table IV) and the full CMB+BAO+RSD+WL+JLA+CC+HST (CBRWJCH in Table IV) we find that the observational constraints are very similar to those obtained for the case with $z_p = 0.05$.

3. Pivoting redshift $z_p = 0.25$

We fix the pivoting redshift to $z_p = 0.25$ and in Table V we summarize the fitting results, while in Fig. 5 we present the corresponding 68% and 95% CL contour plots.

For the case of CMB data only, H_0 is very similar to that obtained for the analysis with $z_p = 0.05$. However, $w_0 < -1$ at more than 68% CL, while in the previous analyses with $z_p = 0.05$ and $z_p = 0.15$ we had found $w_0 > -1$ at 1σ . Additionally, concerning w_a we observe that its mean value lies in the middle between the value obtained for $z_p = 0.05$ and $z_p = 0.15$.

Parameters	CMB	CBR	CBH	CBRWJCH
$\Omega_c h^2$	$0.1191^{+0.0014}_{-0.0014}$	$0.1192^{+0.0013}_{-0.0013}$	$0.1193^{+0.0013}_{-0.0013}$	$0.1183^{+0.0013}_{-0.0013}$
$\Omega_b h^2$	$0.02227^{+0.00015}_{-0.00017}$	$0.02225^{+0.00015}_{-0.00016}$	$0.02226^{+0.00015}_{-0.00015}$	$0.02231^{+0.00015}_{-0.00015}$
$100\theta_{MC}$	$1.04078^{+0.00034}_{-0.00035}$	$1.04076^{+0.00032}_{-0.00032}$	$1.04078^{+0.00032}_{-0.00033}$	$1.04087^{+0.00032}_{-0.00032}$
τ	$0.078^{+0.017}_{-0.017}$	$0.075^{+0.018}_{-0.017}$	$0.077^{+0.017}_{-0.017}$	$0.064^{+0.017}_{-0.017}$
n_s	$0.9665^{+0.0045}_{-0.0046}$	$0.9660^{+0.0043}_{-0.0043}$	$0.9660^{+0.0044}_{-0.0045}$	$0.9675^{+0.0044}_{-0.0043}$
$\ln(10^{10} A_s)$	$3.088^{+0.033}_{-0.034}$	$3.083^{+0.033}_{-0.033}$	$3.088^{+0.034}_{-0.033}$	$3.059^{+0.034}_{-0.034}$
w_0	$-1.40^{+0.28}_{-0.48}$	$-0.827^{+0.084}_{-0.086}$	$-1.074^{+0.079}_{-0.081}$	$-1.007^{+0.041}_{-0.041}$
w_a	$-0.8^{+1.3}_{-0.5}$	$-1.27^{+0.76}_{-0.64}$	$-0.24^{+0.66}_{-0.46}$	$-0.24^{+0.38}_{-0.32}$
Ω_{m0}	$0.229^{+0.043}_{-0.091}$	$0.341^{+0.017}_{-0.019}$	$0.291^{+0.014}_{-0.014}$	$0.3013^{+0.0078}_{-0.0085}$
σ_8	$0.95^{+0.12}_{-0.09}$	$0.804^{+0.016}_{-0.016}$	$0.853^{+0.020}_{-0.020}$	$0.819^{+0.014}_{-0.014}$
H_0	81^{+15}_{-13}	64.6 ± 1.60	70.0 ± 1.7	68.50 ± 0.86
χ^2_{\min} (best-fit)	12959.762	12970.200	12975.904	13722.720

TABLE V: Summary of the 68% CL constraints on the generalized CPL parametrization (7), in the case where the pivoting redshift is fixed at $z_p = 0.25$, using various combinations of the observational data sets. Here, CBR = CMB+BAO+RSD, CBH = CMB+BAO+HST, and CBRWJCH = CMB+BAO+RSD+WL+JLA+CC+HST.

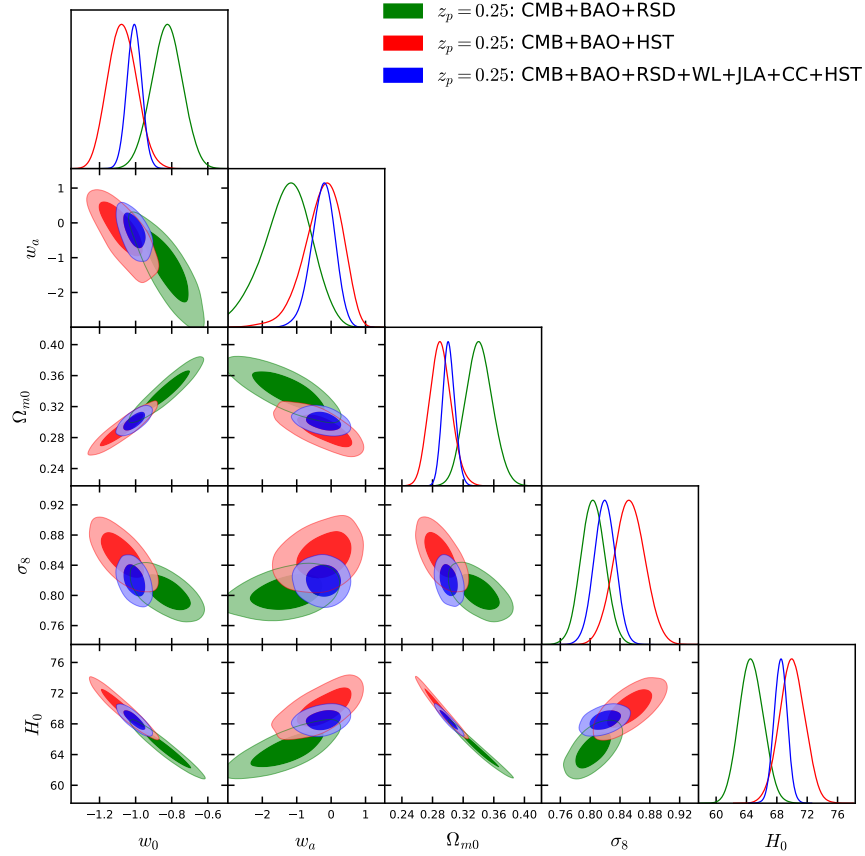


FIG. 5: The 68% and 95% CL 2D contour plots for several combinations of various quantities and using various combinations of the observational data sets, for the generalized CPL parametrization (7) in the case where the pivoting redshift is fixed at $z_p = 0.25$, and the corresponding 1D marginalized posterior distributions.

When we add external data sets to CMB we find significant improvements in the estimations of the Hubble parameter, and its error bars are one order of magnitude smaller. The pattern of the analysis for the combined

dataset CMB+BAO+RSD remains the same as the previous two analyses with the pivoting redshifts $z_p = 0.05$ and $z_p = 0.15$. In fact, w_0 is in the quintessential regime at more than one standard deviation, and the matter

Parameters	CMB	CBR	CBH	CBRWJCH
$\Omega_c h^2$	$0.1190^{+0.0014}_{-0.0014}$	$0.1193^{+0.0013}_{-0.0013}$	$0.1193^{+0.0013}_{-0.0013}$	$0.1183^{+0.0013}_{-0.0012}$
$\Omega_b h^2$	$0.02229^{+0.00016}_{-0.00016}$	$0.02225^{+0.00015}_{-0.00015}$	$0.02226^{+0.00014}_{-0.00016}$	$0.02232^{+0.00015}_{-0.00015}$
$100\theta_{MC}$	$1.04080^{+0.00033}_{-0.00032}$	$1.04076^{+0.00031}_{-0.00032}$	$1.04077^{+0.00032}_{-0.00032}$	$1.04088^{+0.00032}_{-0.00031}$
τ	$0.076^{+0.017}_{-0.017}$	$0.074^{+0.017}_{-0.017}$	$0.078^{+0.017}_{-0.017}$	$0.065^{+0.018}_{-0.017}$
n_s	$0.9666^{+0.0046}_{-0.0049}$	$0.9658^{+0.0044}_{-0.0044}$	$0.9659^{+0.0043}_{-0.0044}$	$0.9678^{+0.0043}_{-0.0044}$
$\ln(10^{10} A_s)$	$3.085^{+0.033}_{-0.033}$	$3.081^{+0.033}_{-0.034}$	$3.089^{+0.034}_{-0.033}$	$3.061^{+0.034}_{-0.033}$
w_0	$-1.40^{+0.23}_{-0.56}$	$-0.903^{+0.055}_{-0.055}$	$-1.083^{+0.061}_{-0.062}$	$-1.022^{+0.033}_{-0.034}$
w_a	-1.0 ± 1.5	$-1.28^{+0.68}_{-0.70}$	$-0.30^{+0.64}_{-0.47}$	$-0.23^{+0.38}_{-0.34}$
Ω_{m0}	$0.239^{+0.040}_{-0.097}$	$0.341^{+0.017}_{-0.017}$	$0.292^{+0.014}_{-0.015}$	$0.3007^{+0.0080}_{-0.0082}$
σ_8	$0.930^{+0.129}_{-0.077}$	$0.804^{+0.016}_{-0.015}$	$0.852^{+0.021}_{-0.020}$	$0.820^{+0.014}_{-0.014}$
H_0	80 ± 13	$64.6^{+1.5}_{-1.6}$	$69.9^{+1.7}_{-1.7}$	$68.55^{+0.86}_{-0.85}$
χ^2_{\min} (best-fit)	12961.850	12969.596	12976.574	13721.112

TABLE VI: Summary of the 68% CL constraints on the generalized CPL parametrization (7), in the case where the pivoting redshift is fixed at $z_p = 0.35$, using various combinations of the observational data sets. Here, CBR = CMB+BAO+RSD, CBH = CMB+BAO+HST, and CBRWJCH = CMB+BAO+RSD+WL+JLA+CC+HST.

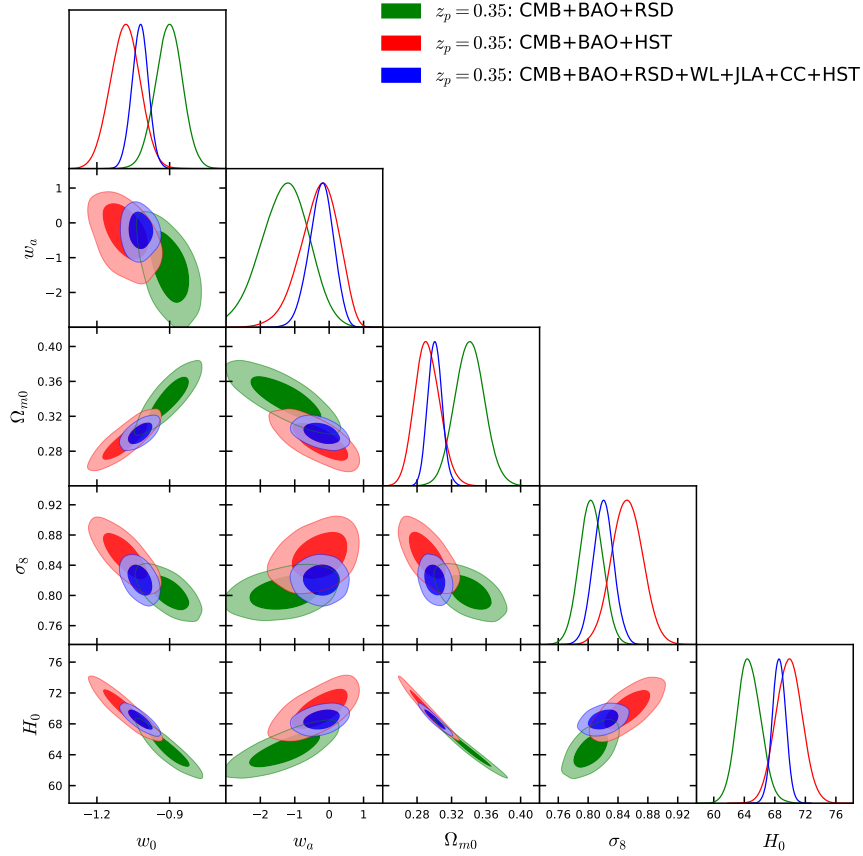


FIG. 6: The 68% and 95% CL 2D contour plots for several combinations of various quantities and using various combinations of the observational data sets, for the generalized CPL parametrization (7) in the case where the pivoting redshift is fixed at $z_p = 0.35$, and the corresponding 1D marginalized posterior distributions.

density parameter shifts towards higher values. A significant improvement appears when we consider the two combinations of data sets, namely, CMB+BAO+HST and CMB+BAO+RSD+WL+JLA+CC+HST, where

the various quantities exhibit similar trends with the previous two fixed pivoting redshifts. We mention that the two key parameters of the dark energy parametrization, namely w_0 and w_a , are now in perfect agreement with

Parameters	CMB	CBR	CBH	CBRWJCH
$\Omega_c h^2$	$0.1189^{+0.0013}_{-0.0013}$	$0.1193^{+0.0013}_{-0.0013}$	$0.1193^{+0.0013}_{-0.0013}$	$0.1182^{+0.0012}_{-0.0012}$
$\Omega_b h^2$	$0.02230^{+0.00015}_{-0.00016}$	$0.02225^{+0.00015}_{-0.00015}$	$0.02226^{+0.00015}_{-0.00015}$	$0.02232657^{+0.00014}_{-0.00015}$
$100\theta_{MC}$	$1.04081^{+0.00033}_{-0.00031}$	$1.04076^{+0.00032}_{-0.00035}$	$1.04078^{+0.00033}_{-0.00031}$	$1.04089^{+0.00031}_{-0.00031}$
τ	$0.078^{+0.019}_{-0.017}$	$0.075^{+0.017}_{-0.017}$	$0.078^{+0.017}_{-0.017}$	$0.066^{+0.016}_{-0.016}$
n_s	$0.9670^{+0.0044}_{-0.0043}$	$0.9659^{+0.0044}_{-0.0044}$	$0.9660^{+0.0043}_{-0.0043}$	$0.9681^{+0.0042}_{-0.0042}$
$\ln(10^{10} A_s)$	$3.088^{+0.036}_{-0.033}$	$3.082^{+0.033}_{-0.032}$	$3.089^{+0.033}_{-0.033}$	$3.061^{+0.032}_{-0.032}$
w_0	$-1.47^{+0.25}_{-0.40}$	$-0.996^{+0.061}_{-0.051}$	$-1.104^{+0.058}_{-0.053}$	$-1.035^{+0.043}_{-0.037}$
w_a	$-0.58^{+0.99}_{-0.35}$	$-1.29^{+0.77}_{-0.65}$	$-0.25^{+0.64}_{-0.49}$	$-0.21^{+0.33}_{-0.32}$
Ω_{m0}	$0.226^{+0.030}_{-0.073}$	$0.341^{+0.018}_{-0.017}$	$0.291^{+0.014}_{-0.015}$	$0.3008^{+0.0077}_{-0.0085}$
σ_8	$0.945^{+0.093}_{-0.071}$	$0.803^{+0.016}_{-0.016}$	$0.853^{+0.020}_{-0.020}$	$0.819^{+0.013}_{-0.014}$
H_0	81^{+10}_{-9}	$64.6^{+1.5}_{-1.7}$	70.0 ± 1.7	$68.52^{+0.85}_{-0.83}$
$\chi^2_{\min} \text{ (best-fit)}$	12960.794	12969.644	12975.328	13723.156

TABLE VII: Summary of the 68% CL constraints on the generalized CPL parametrization (7), in the case where the pivoting redshift is fixed at $z_p = 0.5$, using various combinations of the observational data sets. Here, CBR = CMB+BAO+RSD, CBH = CMB+BAO+HST, and CBRWJCH = CMB+BAO+RSD+WL+JLA+CC+HST.

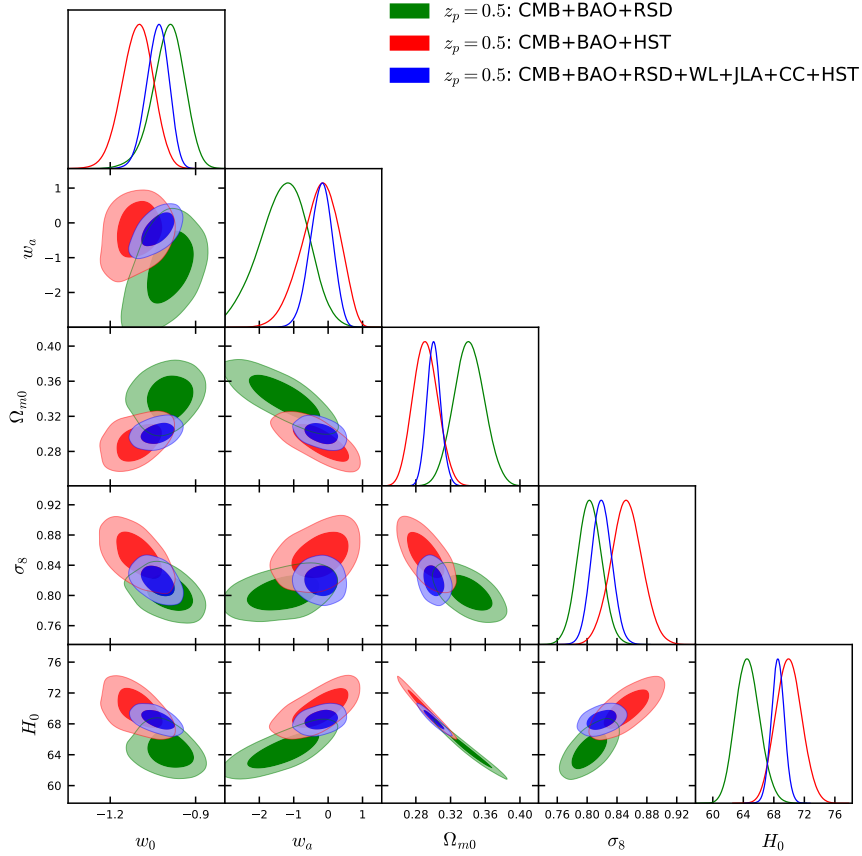


FIG. 7: The 68% and 95% CL 2D contour plots for several combinations of various quantities and using various combinations of the observational data sets, for the generalized CPL parametrization (7) in the case where the pivoting redshift is fixed at $z_p = 0.5$, and the corresponding 1D marginalized posterior distributions.

the cosmological constant.

Parameters	CMB	CBR	CBH	CBRWJCHST
$\Omega_c h^2$	$0.1192^{+0.0014}_{-0.0014}$	$0.1189^{+0.0014}_{-0.0014}$	$0.1192^{+0.0013}_{-0.0014}$	$0.1181^{+0.0012}_{-0.0012}$
$\Omega_b h^2$	$0.02227^{+0.00016}_{-0.00016}$	$0.02228^{+0.00015}_{-0.00016}$	$0.02227^{+0.00015}_{-0.00015}$	$0.02233^{+0.00014}_{-0.00014}$
$100\theta_{MC}$	$1.04079^{+0.00032}_{-0.00033}$	$1.04082^{+0.00033}_{-0.00033}$	$1.04078^{+0.00031}_{-0.00031}$	$1.04089^{+0.00032}_{-0.00031}$
τ	$0.077^{+0.017}_{-0.017}$	$0.076^{+0.018}_{-0.018}$	$0.079^{+0.017}_{-0.017}$	$0.066^{+0.017}_{-0.017}$
n_s	$0.9663^{+0.0049}_{-0.0045}$	$0.9669^{+0.0045}_{-0.0044}$	$0.9661^{+0.0044}_{-0.0044}$	$0.9682^{+0.0043}_{-0.0043}$
$\ln(10^{10} A_s)$	$3.087^{+0.033}_{-0.032}$	$3.083^{+0.035}_{-0.034}$	$3.091^{+0.035}_{-0.033}$	$3.062^{+0.033}_{-0.033}$
w_0	$-1.44^{+0.28}_{-0.42}$	$-1.13^{+0.21}_{-0.11}$	$-1.12^{+0.13}_{-0.08}$	$-1.047^{+0.093}_{-0.053}$
w_a	$-0.6^{+1.0}_{-0.4}$	$-0.88^{+0.98}_{-0.64}$	$-0.12^{+0.61}_{-0.35}$	$-0.11^{+0.37}_{-0.22}$
Ω_{m0}	$0.253^{+0.049}_{-0.094}$	$0.333^{+0.017}_{-0.022}$	$0.289^{+0.012}_{-0.015}$	$0.3001^{+0.0082}_{-0.0083}$
σ_8	0.91 ± 0.10	$0.806^{+0.016}_{-0.016}$	$0.854^{+0.020}_{-0.020}$	$0.819^{+0.013}_{-0.014}$
H_0	77^{+10}_{-13}	65.3 ± 1.8	$70.2^{+1.8}_{-1.6}$	$68.59^{+0.86}_{-0.95}$
χ^2_{\min} (best-fit)	12960.778	12969.896	12975.270	13721.972

TABLE VIII: Summary of the 68% CL constraints on the generalized CPL parametrization (7), in the case where the pivoting redshift is fixed at $z_p = 1$, using various combinations of the observational data sets. Here, CBR = CMB+BAO+RSD, CBH = CMB+BAO+HST, and CBRWJCH = CMB+BAO+RSD+WL+JLA+CC+HST.

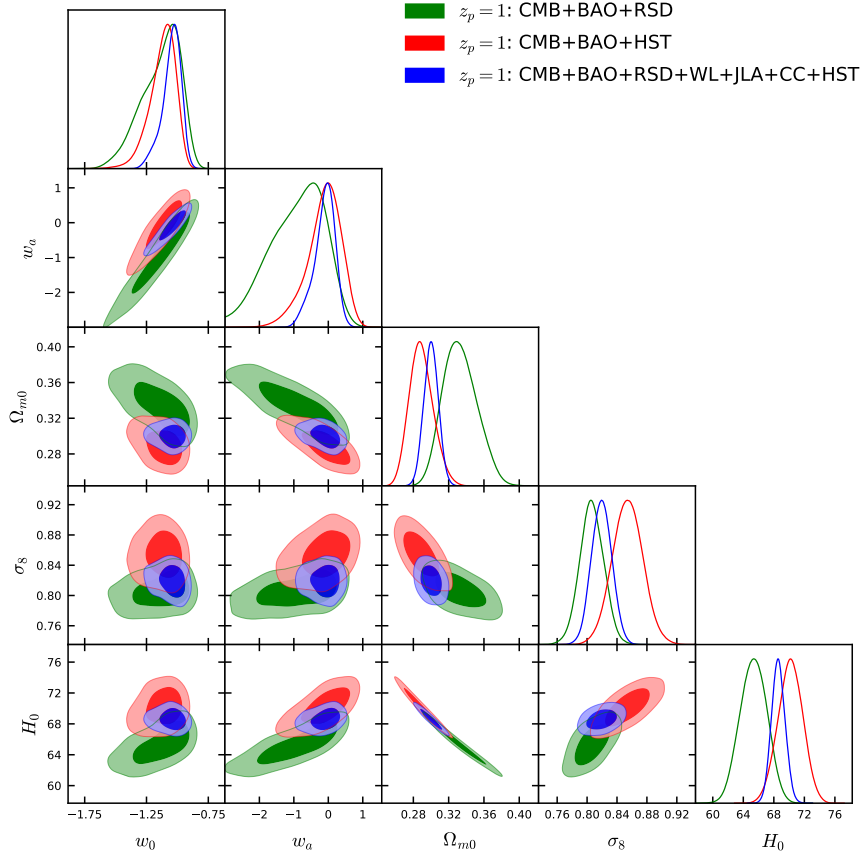


FIG. 8: The 68% and 95% CL 2D contour plots for several combinations of various quantities and using various combinations of the observational data sets, for the generalized CPL parametrization (7) in the case where the pivoting redshift is fixed at $z_p = 1$, and the corresponding 1D marginalized posterior distributions.

4. Pivoting redshift $z_p = 0.35$

We now consider a slightly higher pivot redshift value, namely $z_p = 0.35$, and we summarize the fitting results

in Table VI, while in Fig. 6 we show the corresponding 68% and 95% CL contour plots.

The observational pattern for this parametrization is the same as the previous cases. We find that the CMB

Parameters	CMB	CBR	CBH	CBRWJCH
$\Omega_c h^2$	0.1191 ± 0.0014	$0.1191^{+0.0014}_{-0.0013}$	$0.1192^{+0.0013}_{-0.0012}$	0.1182 ± 0.0012
$\Omega_b h^2$	$0.02228^{+0.00016}_{-0.00015}$	0.02226 ± 0.00015	0.02227 ± 0.00015	0.02233 ± 0.00014
$100\theta_{MC}$	$1.04078^{+0.00031}_{-0.00034}$	$1.04079^{+0.00032}_{-0.00033}$	$1.04079^{+0.00034}_{-0.00031}$	$1.04090^{+0.00031}_{-0.00033}$
τ	0.075 ± 0.017	0.074 ± 0.018	0.079 ± 0.017	0.065 ± 0.016
n_s	0.9664 ± 0.0045	$0.9662^{+0.0044}_{-0.0045}$	$0.9664^{+0.0043}_{-0.0049}$	0.9679 ± 0.0043
$\ln(10^{10} A_s)$	3.084 ± 0.033	$3.080^{+0.035}_{-0.034}$	$3.090^{+0.034}_{-0.033}$	3.060 ± 0.032
w_0	$-1.31^{+0.43}_{-0.56}$	$-0.63^{+0.20}_{-0.30}$	-1.04 ± 0.17	$-0.980^{+0.067}_{-0.085}$
w_a	$-0.9^{+1.0}_{-1.7}$	$-1.1^{+1.0}_{-0.6}$	$-0.18^{+0.56}_{-0.50}$	$-0.16^{+0.31}_{-0.19}$
Ω_{m0}	$0.213^{+0.026}_{-0.077}$	$0.336^{+0.018}_{-0.021}$	$0.290^{+0.014}_{-0.016}$	0.300 ± 0.008
σ_8	$0.968^{+0.118}_{-0.063}$	$0.805^{+0.015}_{-0.015}$	$0.853^{+0.020}_{-0.020}$	$0.819^{+0.014}_{-0.013}$
H_0	84^{+15}_{-8}	$65.0^{+1.8}_{-1.7}$	70.1 ± 1.7	$68.59^{+0.80}_{-0.80}$
χ^2_{\min} (best-fit)	12958.172	12968.590	12976.962	13723.702

TABLE IX: Summary of the 68% CL constraints on the standard CPL parametrization (6), namely without any pivoting redshift ($z_p = 0$), using various combinations of the observational data sets. Here, CBR = CMB+BAO+RSD, CBH = CMB+BAO+HST, and CBRWJCH = CMB+BAO+RSD+WL+JLA+CC+HST.

Datasets	Parameter	z_p free	$z_p = 0$ (CPL)	$z_p = 0.05$	$z_p = 0.15$	$z_p = 0.25$	$z_p = 0.35$	$z_p = 0.5$	$z_p = 1$
CBR	w_0	$-1.33^{+0.35}_{-0.31}$	$-0.63^{+0.20}_{-0.30}$	$-0.68^{+0.24}_{-0.19}$	$-0.78^{+0.12}_{-0.16}$	$-0.827^{+0.084}_{-0.086}$	$-0.903^{+0.055}_{-0.055}$	$-0.996^{+0.061}_{-0.051}$	$-1.13^{+0.21}_{-0.11}$
CBR	w_a	$-1.21^{+0.62}_{-0.62}$	$-1.1^{+1.0}_{-0.6}$	$-1.10^{+0.70}_{-0.92}$	$-1.05^{+0.92}_{-0.59}$	$-1.27^{+0.76}_{-0.64}$	$-1.28^{+0.68}_{-0.70}$	$-1.29^{+0.77}_{-0.65}$	$-0.88^{+0.98}_{-0.64}$
CBRWJCH	w_0	$-1.11^{+0.17}_{-0.11}$	$-0.980^{+0.067}_{-0.085}$	$-1.001^{+0.061}_{-0.078}$	$-1.010^{+0.045}_{-0.053}$	$-1.007^{+0.041}_{-0.041}$	$-1.022^{+0.033}_{-0.034}$	$-1.035^{+0.043}_{-0.037}$	$-1.047^{+0.093}_{-0.053}$
CBRWJCH	w_a	$-0.24^{+0.38}_{-0.33}$	$-0.16^{+0.31}_{-0.19}$	$-0.09^{+0.32}_{-0.20}$	$-0.09^{+0.30}_{-0.19}$	$-0.24^{+0.38}_{-0.32}$	$-0.23^{+0.38}_{-0.34}$	$-0.21^{+0.33}_{-0.32}$	$-0.11^{+0.37}_{-0.22}$

TABLE X: Summary of the constraints on the dark energy parametrization (7), for various values of the pivot redshift z_p (free/fixed), using the observational data CBR = CMB+BAO+RSD (upper half of the table) and CBRWJCH = CMB+BAO+RSD+WL+JLA+CC+HST (lower half of the table).

data only constrain $w_0 < -1$ at more than 68% CL, and we recover the cosmological constant scenario as soon as we add more external datasets to CMB. In this case, it appears an indication for $w_0 < -1$ at one standard deviation also for the CMB+BAO+HST case. Moreover, the results with the full combination of datasets are very stable and robust towards changing the fixed pivot redshift.

5. Pivoting redshift $z_p = 0.5$

For the case $z_p = 0.50$, we summarize the fitting results in Table VII and in Fig. 7 we present the corresponding 68% and 95% CL contour plots. As we see, the constraints on the parameters are very similar to the case $z_p = 0.35$. In particular, we have the preference for a phantom regime at one standard deviation for the CMB and the CMB+BAO+HST cases, while on the other hand for the combinations CMB+BAO+RSD and CMB+BAO+RSD+WL+JLA+CC+HST the parametrization is in agreement with the cosmological constant.

6. Pivoting redshift $z_p = 1$

Finally, we consider the last fixed pivoting redshift in this series, namely $z_p = 1$. In Table VIII we summarize the fitting results while in Fig. 8 we depict the corresponding 68% and 95% CL contour plots. The overall results are similar with respect to the previous fixed pivot redshift cases, however one can clearly see that for CMB+BAO+RSD data sets w_0 has a mean value in the phantom regime ($w_0 = -1.13^{+0.21}_{-0.11}$ at 68% CL). Therefore, with the increment of the pivoting redshift we find a successive change in the estimation of w_0 . One can further notice that for the CMB data only $w_0 < -1$ is always favored, but all the other combinations of data recover the cosmological constant within 68% CL.

V. STATISTICAL COMPARISON OF ALL PARAMETRIZATIONS

In this section we proceed to a comparison of the various generalized CPL parametrizations, with and without the pivoting redshift. Hence, for completeness we perform a similar observational confrontation with the previous section for the standard CPL parametrization, namely without pivoting redshift (i.e. $z_p = 0$), and we summarize the results in Table IX.

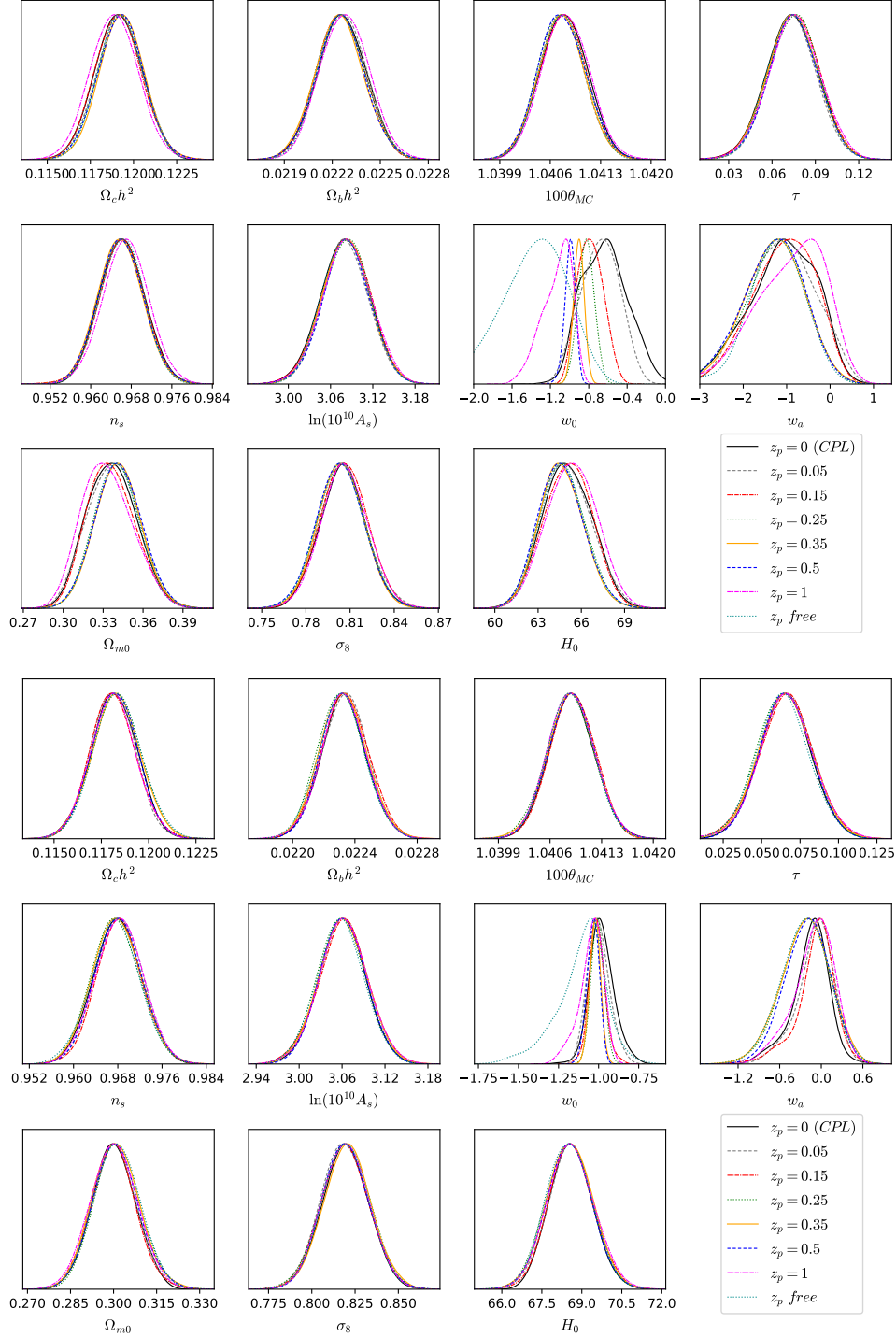


FIG. 9: One-dimensional marginalized posterior distributions of various parameters of the generalized CPL parametrization, for free and fixed pivoting redshift z_p , for the combined analyses CMB+BAO+RSD (upper three rows) and CMB+BAO+RSD+WL+JLA+CC+HST (lower three rows). One can observe that the various parameters behave similarly, apart from w_0 and w_a .

We can now perform the model comparison following the summarizing Tables given above, namely Table II (varying z_p), Table III ($z_p = 0.05$), Table IV ($z_p = 0.15$), Table V ($z_p = 0.25$), Table VI ($z_p = 0.35$), Table VII

($z_p = 0.5$), Table VIII ($z_p = 1$), and Table IX (no pivoting redshift, i.e. $z_p = 0$).

First of all, from all the analyses we find that the CMB data alone do not provide stringent constraints

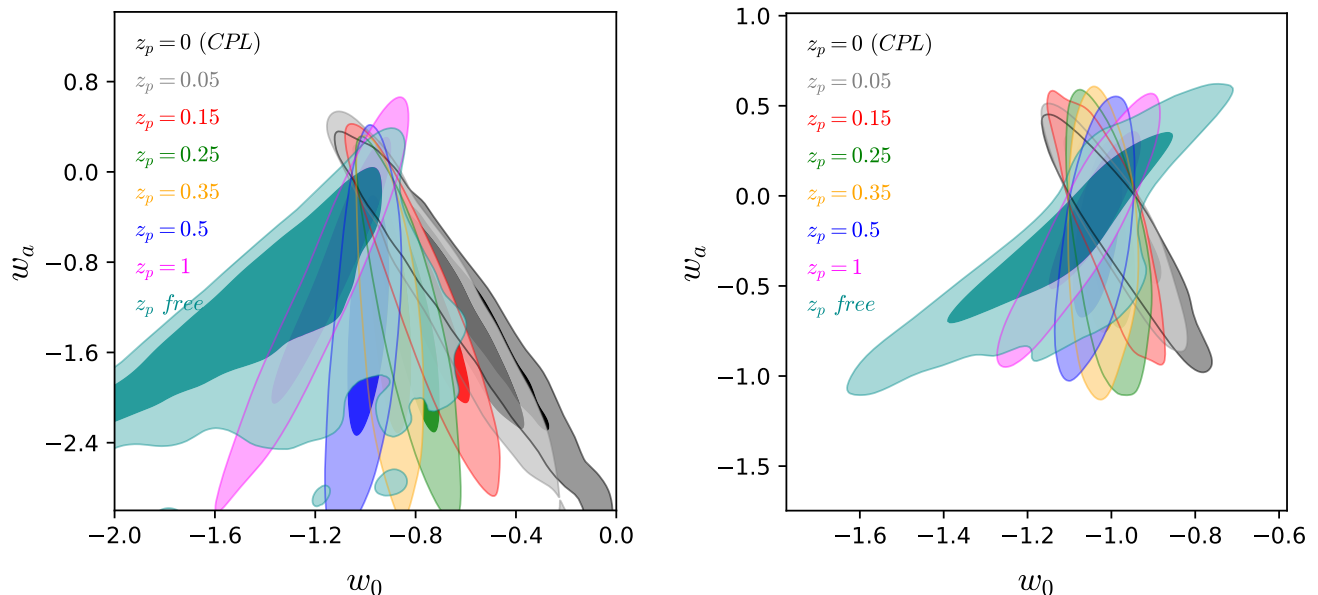


FIG. 10: The 68% and 95% CL contour plots in the $w_0 - w_a$ plane, for the generalized CPL parametrization (7) for various pivoting redshifts z_p , and for the data combinations CMB+BAO+RSD (left graph) and CMB+BAO+RSD+WL+JLA+CC+HST (right graph).

on the free parameters, however, we observe that the addition of any external datasets leads to a refinement of the constraints by reducing their error bars in a significant way. Furthermore, we find that the CMB+BAO+RSD combination returns slightly different constraints compared to the remaining two datasets, nevertheless for this combination we find an interesting pattern in the w_0 parameter, where we observe that with increasing z_p , w_0 eventually approaches towards the cosmological constant value and finally for large z_p ($z_p = 1$) it crosses the -1 boundary. Concerning the remaining two datasets, namely CMB+BAO+HST and CMB+BAO+RSD+WL+JLA+CC+HST, we find that the cosmological constraints are similar, with the best constraints definitely achieved for the final combination. Thus, in this section we focus on the observational datasets CMB+BAO+RSD and CMB+BAO+RSD+WL+JLA+CC+HST, in order to provide a statistical comparison between the cosmological models for free and fixed pivoting redshift z_p .

In order to proceed towards the statistical comparisons of the models, in Table X we depict the constraints on the basic model parameters for different values of z_p (free and fixed). Furthermore, in Fig. 9 we present the one-dimensional marginalized posterior distributions for the free parameters. In particular, the upper part of Fig. 9 corresponds to the CMB+BAO+RSD dataset, while the lower part to the full combination CMB+BAO+RSD+WL+JLA+CC+HST. From both parts of Fig. 9 we can clearly notice that all parameters present the same behavior independently of the pivoting redshift z_p , apart from w_0 and w_a .

Hence, in order to examine in more detail the effect of z_p on w_0, w_a , in Fig. 10 we depict the contour plots in the $w_0 - w_a$ plane for various z_p , for the combinations CMB+BAO+RSD (left panel of Fig. 10) and CMB+BAO+RSD+WL+JLA+CC+HST (right panel of Fig. 10).

As we observe in Fig. 10 for both datasets, by changing the values of z_p the correlations between w_0 and w_a change significantly. In particular, starting from a negative correlation present for $z_p = 0$ (the original CPL parametrization), increasing the z_p values leads to a rotation of the direction of the degeneracy between these two parameters. Therefore, we find a positive correlation for $z_p = 1$, as well as in the case where z_p is left free. Finally, we can identify the value of the pivoting redshift for which w_0 and w_a are no more correlated, and this is approximately $z_p = 0.35$ for both datasets (the contours corresponding to $z_p = 0.35$ (yellow) are vertical, showing no degeneracy). The changing of the correlations from negative to positive is one of the main results of this work.

Lastly, in order to provide the obtained results in a more transparent way, in Fig. 11 we provide the whisker plot for the equation-of-state parameter at present, namely w_0 , for all the examined cases of the generalized CPL parametrization. As we observe, although the constraints for all data combinations behave in a stable way, the increase in z_p pushes w_0 towards the phantom regime.

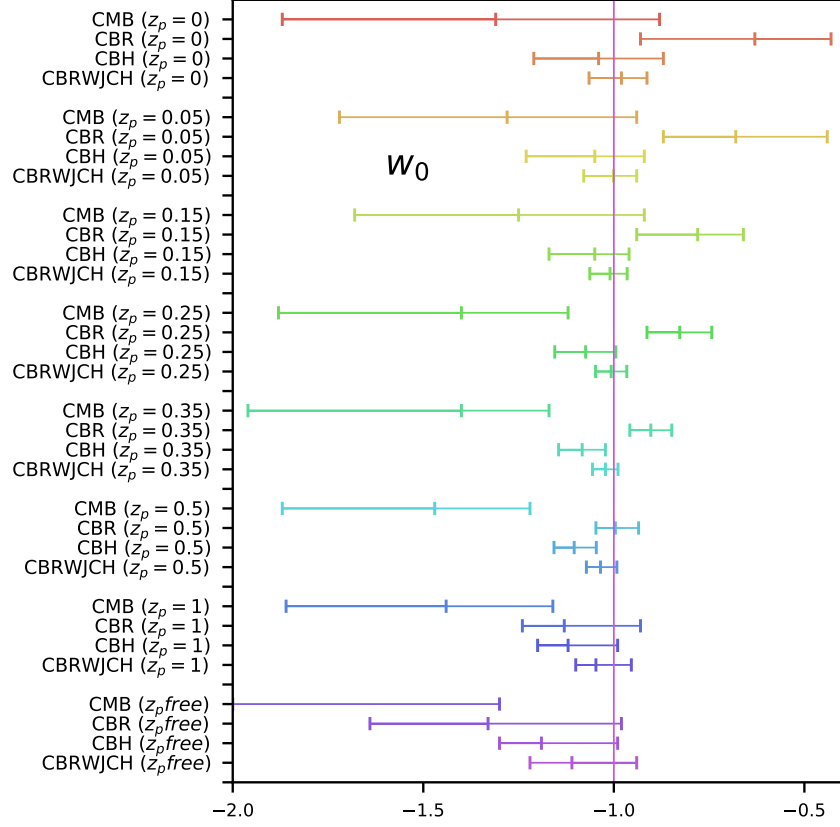


FIG. 11: Whisker plot for the present value of the equation-of-state parameter, w_0 , for all the examined cases of the generalized CPL parametrization (7). Here, CBR = CMB+BAO+RSD, CBH = CMB+BAO+HST, and CBRWJCH = CMB+BAO+RSD+WL+JLA+CC+HST.

VI. CONCLUDING REMARKS

Dynamical dark energy parametrizations are an effective approach to understand the evolution of the universe, without needing to know the microphysical origin of the dark-energy and whether it corresponds to new fields or to gravitational modification. Hence, a large number of such dark-energy equation-of-state parametrizations have been introduced in the literature, with the Chevallier-Polarski-Linder (CPL) being one of the most studied.

Nevertheless, in most of the above parametrizations one considers the “pivoting redshift” z_p to correspond to zero, namely the point at which the dark-energy equation-of-state is most tightly constrained to correspond to the current universe. However, in the case of two-parameter models, due to possible rotational correlations between the two parameters, in principle one could avoid setting the pivoting redshift to zero straightaway,

handling it as a free parameter.

In the present work we investigated the observational constraints on such a generalized CPL parametrization, namely incorporating the pivoting redshift as an extra parameter, assuming it to be either fixed or free. For this shake we used various data combinations from cosmic microwave background (CMB), baryon acoustic oscillations (BAO), redshift space distortion (RSD), weak lensing (WL), joint light curve analysis (JLA), cosmic chronometers (CC), and we additionally included a Gaussian prior on the Hubble constant value. We considered two different cases, namely one in which z_p is handled as a free parameter, and one in which it is fixed to a specific value. For the later case we considered various values of $z_p \in [0, 1]$, in order to examine how the fixed z_p value affects the results.

For the case of free z_p , we found that for all data combinations it always remains unconstrained, and there is a degeneracy with the current value of the dark energy

equation of state w_0 (see Fig. 2). On the other hand, in the case where z_p is fixed we did not find any degeneracy in the parameter space, as expected. In particular, the mean values of w_0 lie always in the phantom regime, and for higher values of z_p (0.25, 0.35, 0.5, 1), $w_0 < -1$ at more than 1σ while for lower values of z_p ($z_p = 0, 0.05, 0.15$) the quintessence regime is also allowed at 1σ .

The inclusion of any external data set to sole CMB data, such as BAO+RSD, BAO+HST, and BAO+RSD+WL+JLA+CC+HST, significantly improves the CMB constraints by reducing the error bars on the various quantities. For instance, irrespectively of the different fixed z_p values, the CMB data always return high values for the present Hubble constant H_0 with large error bars, which both decrease for the combined data cases.

Concerning the constraints on w_0 , for the CMB+BAO+RSD dataset we saw that they depend on the values of z_p . In particular, for low z_p ($z_p = 0.05, 0.15, 0.25, 0.35, 0.5$) the mean values of w_0 are always quintessential, while for $z_p = 1$ the mean value of w_0 lies in the phantom regime. Nevertheless, a common characteristic is that for all z_p values $w_0 > -1$ is allowed within 68% CL (note that for $z_p = 0.05, 0.15, 0.25, 0.35$ within 68% CL w_0 is strictly greater than -1). Furthermore, for the CMB+BAO+HST dataset we saw that the obtained w_0 -values for different z_p are in better agreement with the cosmological constant. Additionally, for the last full combination of CMB+BAO+RSD+WL+JLA+CC+HST, we also found

that w_0 is consistent with the cosmological constant, independently of the z_p values. As expected, compared to all the analyses performed in this work, the cosmological constraints obtained for the full data combination, namely CMB+BAO+RSD+WL+JLA+CC+HST, are much more stringent, as it was summarized in the whisker plot of Fig. 11.

Finally, in the above analysis we were able to reveal a correlation between the parameters w_0 and w_a for different z_p (see Fig. 10). In particular, we found that with increasing z_p the correlations between w_0 and w_a change from negative to positive (the direction of degeneracy is rotating from negative to positive), and for the case $z_p = 0.35$, w_0 and w_a are uncorrelated. This is one of the main results of the present work, and indeed it justifies why a non-zero pivoting redshift should be taken into account.

Acknowledgments

WY has been supported by the National Natural Science Foundation of China under Grants No. 11705079 and No. 11647153. SP and WY thank G. Pantazis for many discussions. EDV acknowledges support from the European Research Council in the form of a Consolidator Grant with number 681431. This article is based upon work from CANTATA COST (European Cooperation in Science and Technology) action CA15117, EU Framework Programme Horizon 2020.

-
- [1] E. J. Copeland, M. Sami and S. Tsujikawa, *Dynamics of dark energy*, Int. J. Mod. Phys. D **15**, 1753 (2006).
 - [2] Y. F. Cai, E. N. Saridakis, M. R. Setare and J. Q. Xia, *Quintom Cosmology: Theoretical implications and observations*, Phys. Rept. **493**, 1 (2010).
 - [3] S. Nojiri and S. D. Odintsov, *Introduction to modified gravity and gravitational alternative for dark energy*, eConf C **0602061**, 06 (2006) [Int. J. Geom. Meth. Mod. Phys. **4**, 115 (2007)].
 - [4] A. De Felice and S. Tsujikawa, *$f(R)$ theories*, Living Rev. Rel. **13**, 3 (2010).
 - [5] S. Capozziello and M. De Laurentis, *Extended Theories of Gravity*, Phys. Rept. **509**, 167 (2011).
 - [6] Y. F. Cai, S. Capozziello, M. De Laurentis and E. N. Saridakis, *$f(T)$ teleparallel gravity and cosmology*, Rept. Prog. Phys. **79**, no. 10, 106901 (2016).
 - [7] S. Nojiri, S. D. Odintsov and V. K. Oikonomou, *Modified Gravity Theories on a Nutshell: Inflation, Bounce and Late-time Evolution*, Phys. Rept. **692**, 1 (2017).
 - [8] Y. g. Gong and Y. Z. Zhang, *Probing the curvature and dark energy*, Phys. Rev. D **72**, 043518 (2005).
 - [9] W. Yang, S. Pan, E. Di Valentino, E. N. Saridakis and S. Chakraborty, *Observational constraints on one-parameter dynamical dark-energy parametrizations and the H_0 tension*, arXiv:1810.05141 [astro-ph.CO].
 - [10] M. Chevallier and D. Polarski, *Accelerating universes with scaling dark matter*, Int. J. Mod. Phys. D **10**, 213 (2001).
 - [11] E. V. Linder, *Exploring the expansion history of the universe*, Phys. Rev. Lett. **90**, 091301 (2003).
 - [12] A. R. Cooray and D. Huterer, *Gravitational lensing as a probe of quintessence*, Astrophys. J. **513**, L95 (1999).
 - [13] P. Astier, *Can luminosity distance measurements probe the equation of state of dark energy*, Phys. Lett. B **500**, 8 (2001).
 - [14] J. Weller and A. Albrecht, *Future supernovae observations as a probe of dark energy*, Phys. Rev. D **65**, 103512 (2002).
 - [15] G. Efstathiou, *Constraining the equation of state of the universe from distant type Ia supernovae and cosmic microwave background anisotropies*, Mon. Not. Roy. Astron. Soc. **310**, 842 (1999).
 - [16] H. K. Jassal, J. S. Bagla and T. Padmanabhan, *Observational constraints on low redshift evolution of dark energy: How consistent are different observations?*, Phys. Rev. D **72**, 103503 (2005).
 - [17] E. M. Barboza, Jr. and J. S. Alcaniz, *A parametric model for dark energy*, Phys. Lett. B **666**, 415 (2008).
 - [18] J. Z. Ma and X. Zhang, *Probing the dynamics of dark energy with novel parametrizations*, Phys. Lett. B **699**, 233 (2011).
 - [19] S. Nesseris and L. Perivolaropoulos, *A Comparison of*

- cosmological models using recent supernova data, *Phys. Rev. D* **70**, 043531 (2004).
- [20] E. V. Linder and D. Huterer, *How many dark energy parameters?*, *Phys. Rev. D* **72**, 043509 (2005).
- [21] B. Feng, M. Li, Y. S. Piao and X. Zhang, *Oscillating quintom and the recurrent universe*, *Phys. Lett. B* **634**, 101 (2006).
- [22] G. B. Zhao, J. Q. Xia, H. Li, C. Tao, J. M. Virey, Z. H. Zhu and X. Zhang, *Probing for dynamics of dark energy and curvature of universe with latest cosmological observations*, *Phys. Lett. B* **648**, 8 (2007).
- [23] S. Nojiri and S. D. Odintsov, *The Oscillating dark energy: Future singularity and coincidence problem*, *Phys. Lett. B* **637**, 139 (2006).
- [24] E. N. Saridakis, *Theoretical Limits on the Equation-of-State Parameter of Phantom Cosmology*, *Phys. Lett. B* **676**, 7 (2009).
- [25] S. Dutta, E. N. Saridakis and R. J. Scherrer, *Dark energy from a quintessence (phantom) field rolling near potential minimum (maximum)*, *Phys. Rev. D* **79**, 103005 (2009).
- [26] R. Lazkoz, V. Salzano and I. Sendra, *Oscillations in the dark energy EoS: new MCMC lessons*, *Phys. Lett. B* **694**, 198 (2011).
- [27] L. Feng and T. Lu, *A new equation of state for dark energy model*, *JCAP* **1111**, 034 (2011).
- [28] E. N. Saridakis, *Phantom evolution in power-law potentials*, *Nucl. Phys. B* **819**, 116 (2009).
- [29] A. De Felice, S. Nesseris and S. Tsujikawa, *Observational constraints on dark energy with a fast varying equation of state*, *JCAP* **1205**, 029 (2012).
- [30] E. N. Saridakis, *Quintom evolution in power-law potentials*, *Nucl. Phys. B* **830**, 374 (2010).
- [31] C. J. Feng, X. Y. Shen, P. Li and X. Z. Li, *A New Class of Parametrization for Dark Energy without Divergence*, *JCAP* **1209**, 023 (2012).
- [32] S. Basilakos and J. Solá, *Effective equation of state for running vacuum: mirage quintessence and phantom dark energy*, *Mon. Not. Roy. Astron. Soc.* **437**, no. 4, 3331 (2014).
- [33] G. Pantazis, S. Nesseris and L. Perivolaropoulos, *Comparison of thawing and freezing dark energy parametrizations*, *Phys. Rev. D* **93**, no. 10, 103503 (2016).
- [34] E. Di Valentino, A. Melchiorri and J. Silk, *Reconciling Planck with the local value of H_0 in extended parameter space*, *Phys. Lett. B* **761**, 242 (2016).
- [35] R. Chávez, M. Plionis, S. Basilakos, R. Terlevich, E. Terlevich, J. Melnick, F. Bresolin and A. L. González-Morán, *Constraining the dark energy equation of state with HII galaxies*, *Mon. Not. Roy. Astron. Soc.* **462**, no. 3, 2431 (2016).
- [36] G. B. Zhao *et al.*, *Dynamical dark energy in light of the latest observations*, *Nat. Astron.* **1**, 627 (2017).
- [37] W. Yang, R. C. Nunes, S. Pan and D. F. Mota, *Effects of neutrino mass hierarchies on dynamical dark energy models*, *Phys. Rev. D* **95**, 103522 (2017).
- [38] E. Di Valentino, A. Melchiorri, E. V. Linder and J. Silk, *Constraining Dark Energy Dynamics in Extended Parameter Space*, *Phys. Rev. D* **96**, 023523 (2017).
- [39] E. Di Valentino, *Crack in the cosmological paradigm*, *Nat. Astron.* **1**, 569 (2017).
- [40] W. Yang, S. Pan and A. Paliathanasis, *Latest astronomical constraints on some nonlinear parametric dark energy models*, *Mon. Not. Roy. Astron. Soc.* **475**, 2605 (2018).
- [41] R. J. F. Marcondes and S. Pan, *Cosmic chronometers constraints on some fast-varying dark energy equations of state*, arXiv:1711.06157 [astro-ph.CO].
- [42] S. Pan, E. N. Saridakis and W. Yang, *Observational Constraints on Oscillating Dark-Energy Parametrizations*, *Phys. Rev. D* **98**, no. 6, 063510 (2018).
- [43] E. V. Linder, *Biased Cosmology: Pivots, Parameters, and Figures of Merit*, *Astropart. Phys.* **26**, 102 (2006).
- [44] V. Sahni and A. Starobinsky, *Reconstructing Dark Energy*, *Int. J. Mod. Phys. D* **15**, 2105 (2006).
- [45] D. Scovacricchi, S. A. Bonometto, M. Mezzetti and G. La Vacca, *Constraints on Dark Energy state equation with varying pivoting redshift*, *New Astron.* **26**, 106 (2014).
- [46] V. F. Mukhanov, H. A. Feldman and R. H. Brandenberger, *Theory of cosmological perturbations*, *Phys. Rept.* **215**, 203 (1992).
- [47] C. P. Ma and E. Bertschinger, *Cosmological perturbation theory in the synchronous and conformal Newtonian gauges*, *Astrophys. J.* **455**, 7 (1995).
- [48] K. A. Malik and D. Wands, *Cosmological perturbations*, *Phys. Rept.* **475**, 1 (2009).
- [49] R. Adam *et al.* [Planck Collaboration], *Planck 2015 results. I. Overview of products and scientific results*, *Astron. Astrophys.* **594**, A1 (2016).
- [50] N. Aghanim *et al.* [Planck Collaboration], *Planck 2015 results. XI. CMB power spectra, likelihoods, and robustness of parameters*, *Astron. Astrophys.* **594**, A11 (2016).
- [51] Y. Akrami *et al.* [Planck Collaboration], *Planck 2018 results. I. Overview and the cosmological legacy of Planck*, arXiv:1807.06205 [astro-ph.CO].
- [52] N. Aghanim *et al.* [Planck Collaboration], *Planck 2018 results. VI. Cosmological parameters*, arXiv:1807.06209 [astro-ph.CO].
- [53] P. A. R. Ade *et al.* [Planck Collaboration], *Planck 2015 results. XIII. Cosmological parameters*, arXiv:1502.01589 [astro-ph.CO].
- [54] F. Beutler *et al.*, *The 6dF Galaxy Survey: Baryon Acoustic Oscillations and the Local Hubble Constant*, *Mon. Not. Roy. Astron. Soc.* **416**, 3017 (2011).
- [55] A. J. Ross, L. Samushia, C. Howlett, W. J. Percival, A. Burden and M. Manera, *The clustering of the SDSS DR7 main Galaxy sample I. A 4 per cent distance measure at $z = 0.15$* , *Mon. Not. Roy. Astron. Soc.* **449**, no. 1, 835 (2015).
- [56] H. Gil-Marín *et al.*, *The clustering of galaxies in the SDSS-III Baryon Oscillation Spectroscopic Survey: BAO measurement from the LOS-dependent power spectrum of DR12 BOSS galaxies*, *Mon. Not. Roy. Astron. Soc.* **460**, no. 4, 4210 (2016).
- [57] H. Gil-Marín *et al.*, *The clustering of galaxies in the SDSS-III Baryon Oscillation Spectroscopic Survey: RSD measurement from the power spectrum and bispectrum of the DR12 BOSS galaxies*, *Mon. Not. Roy. Astron. Soc.* **465**, no.2, 1757 (2017).
- [58] C. Heymans *et al.*, *CFHTLenS tomographic weak lensing cosmological parameter constraints: Mitigating the impact of intrinsic galaxy alignments*, *Mon. Not. Roy. Astron. Soc.* **432**, 2433 (2013).
- [59] T. Erben *et al.*, *CFHTLenS: The Canada-France-Hawaii Telescope Lensing Survey - Imaging Data and Catalogue Products*, *Mon. Not. Roy. Astron. Soc.* **433**, 2545 (2013).
- [60] M. Asgari, C. Heymans, C. Blake, J. Harnois-Deraps, P. Schneider and L. Van Waerbeke, *Revisiting CFHTLenS cosmic shear: Optimal E/B mode decomposition using COSEBIs and compressed COSEBIs*, *Mon.*

- Not. Roy. Astron. Soc. **464**, 1676 (2017).
- [61] M. Betoule *et al.* [SDSS Collaboration], *Improved cosmological constraints from a joint analysis of the SDSS-II and SNLS supernova samples*, Astron. Astrophys. **568**, A22 (2014).
 - [62] M. Moresco *et al.*, *A 6% measurement of the Hubble parameter at $z \sim 0.45$: direct evidence of the epoch of cosmic re-acceleration*, JCAP **1605**, 014 (2016).
 - [63] A. G. Riess *et al.*, *A 2.4% Determination of the Local Value of the Hubble Constant*, Astrophys. J. **826**, no. 1, 56 (2016).
 - [64] A. Lewis and S. Bridle, “*Cosmological parameters from CMB and other data: A Monte Carlo approach*,” Phys. Rev. D **66**, 103511 (2002).
 - [65] A. Gelman and D. Rubin, *Inference from iterative simulation using multiple sequences*, Statistical Science **7**, 457 (1992).
 - [66] A. Lewis, *Efficient sampling of fast and slow cosmological parameters*, Phys. Rev. D **87**, no. 10, 103529 (2013).
 - [67] P. A. R. Ade *et al.* [Planck Collaboration], *Planck 2015 results. XIII. Cosmological parameters*, Astron. Astrophys. **594**, A13 (2016).